Supplementary Materials

Bioinspired Camouflage Fibers with Computer Vision-Guided Chromatic Adaptation

Luyao Huang[1, 5], Tingyu Cheng[2], Xianzhe Zhang[3], Haichao Zhang[3], Tejonidhi Deshpande[2], Yuanqiao Li[4], Zhi Xu[3], Gregory D. Abowd[2, 3], Yun Fu[3, 4], Yongmin Liu[3], Josiah Hester[2], Jun Li[5], Hongli Zhu[1*]

[1] Department of Mechanical and Industrial Engineering, Northeastern University, Boston, MA 02115, USA

[2] College of Computing, Georgia Institute of Technology, Atlanta, GA 30332, USA

[3] Department of Electrical and Computer Engineering, Northeastern University, Boston, MA, 02115, USA Georgia Institute of Technology

[4] Khoury College of Computer Sciences, Northeastern University, Boston, MA, 02115, USA

[5] State Key Laboratory of Advanced Papermaking and Paper-based Materials, South China University of Technology, Guangzhou, 510640, China

This PDF file includes:

Figs. S1 to S3

Tables S1 to S3

Legends for movies S1 to S7

Other Supplementary Material for this manuscript includes the following:

Movies S1 to S7

The PDMS transparent tubes were prepared according to a cure ratio of 11:1. The resulting PDMS tubes had a wall thickness of 0.3 mm and an inner diameter of 1.0 mm.

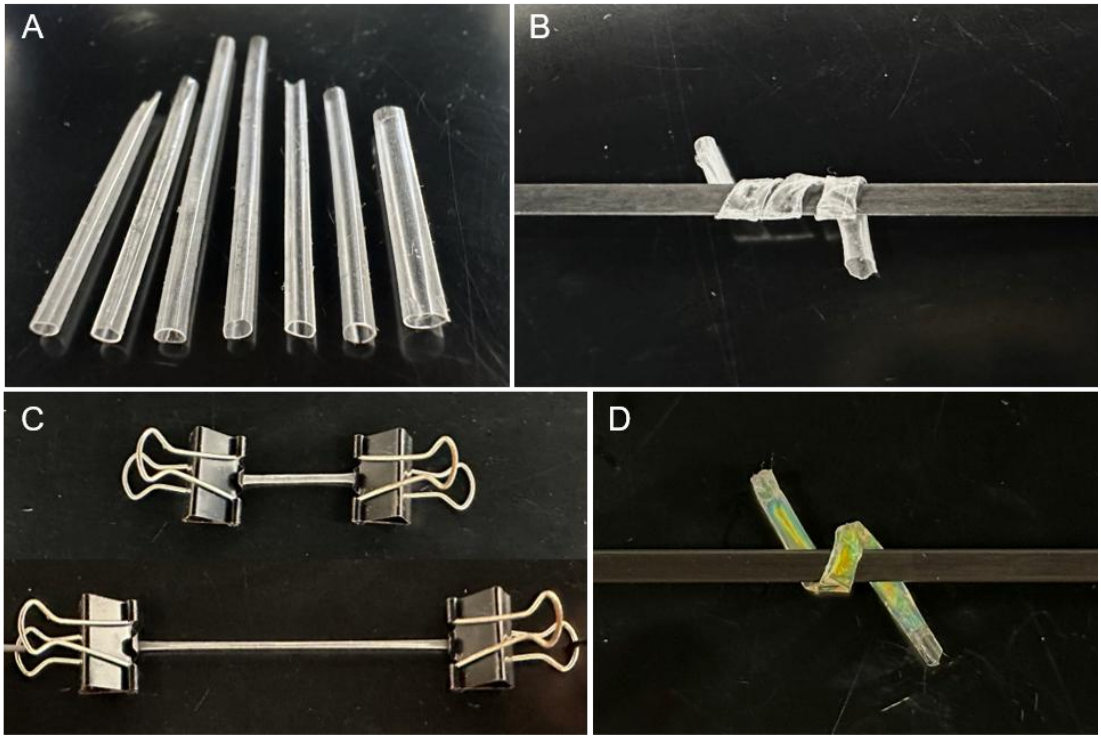

Fig. S1. Mechanical as well as optical properties of PDMS transparent tubes.

(A) PDMS transparent tubes; (B) the bendability and crimp ability of PDMS tubes; (C) the stretchability of PDMS tubes; (D) the bendability and crimp ability of PDMS tubes loaded with HPC gel.

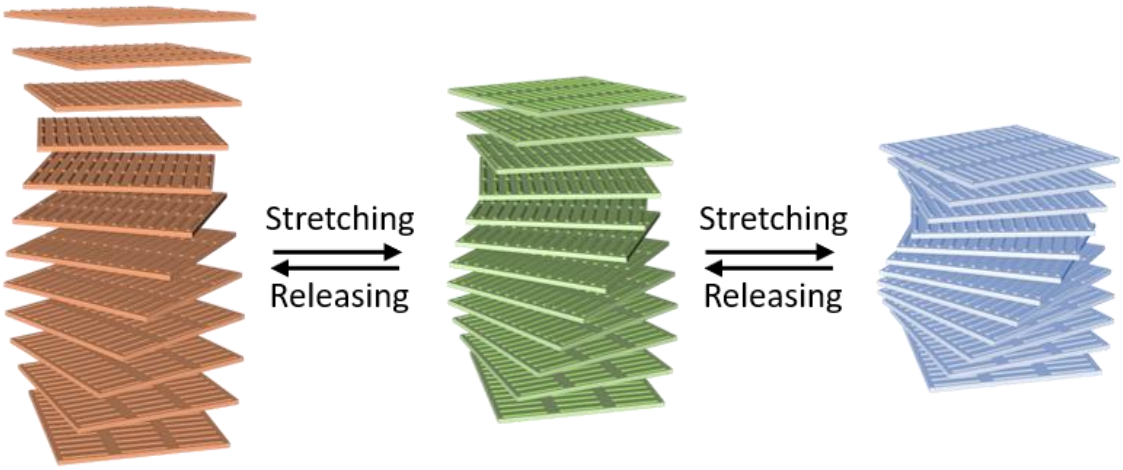

Fig. S2. The alteration in the periodic structure of HPC under stretch or release.

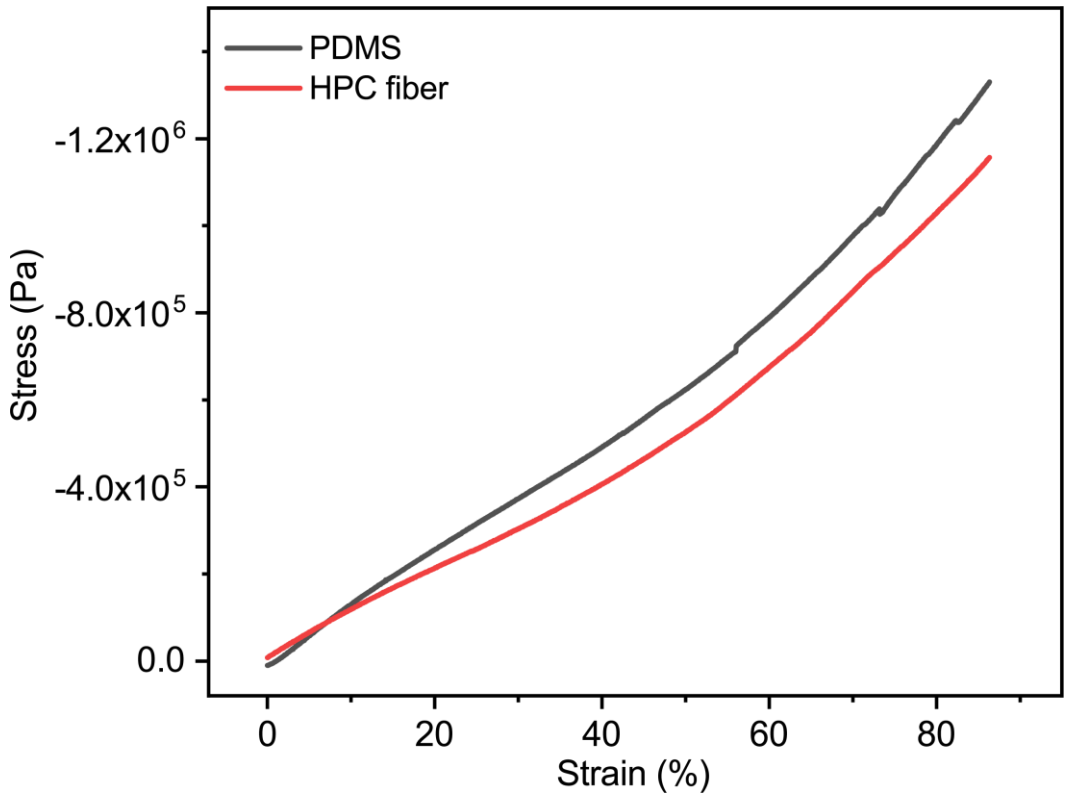

Fig. S3. Stress-strain curves of PDMS transparent tubes and HPC fiber.

The tensile tests reveal a Young's modulus of approximately 14,052 Pa for PDMS tubes and 11,627 Pa for HPC fibers. The mechanical flexibility of the HPC fibers enables reliable deformation and recovery during actuation cycles, supporting the durability of the camouflage mechanism.

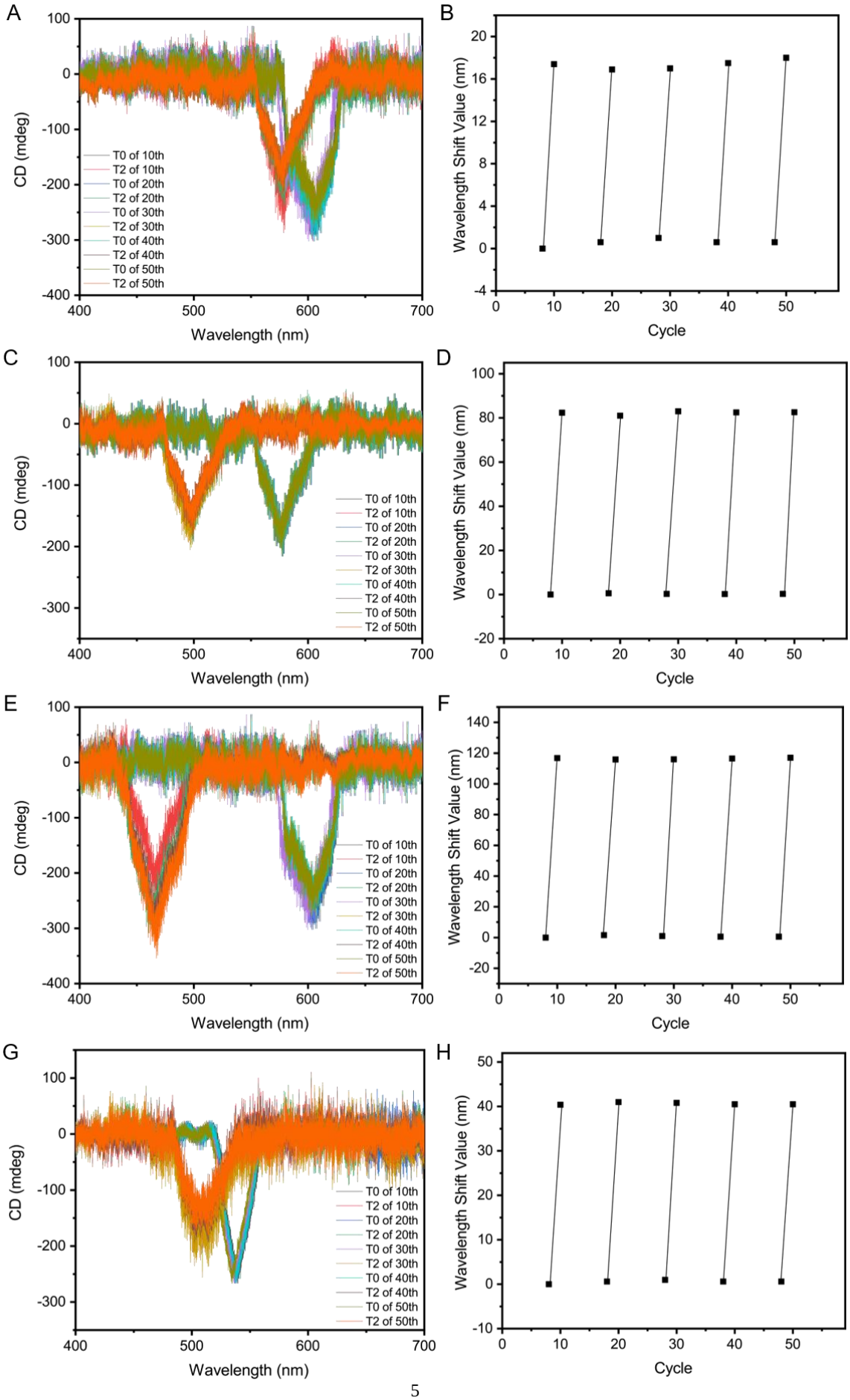
A
CD (mdeg)
Wavelength (nm)
T0 of 10th
T2 of 10th
T0 of 20th
T2 of 20th
T0 of 30th
T2 of 30th
T0 of 40th
T2 of 40th
T0 of 50th
T2 of 50th
B
Wavelength Shift Value (nm)
Cycle
C
CD (mdeg)
Wavelength (nm)
D
Wavelength Shift Value (nm)
Cycle
E
CD (mdeg)
Wavelength (nm)
F
Wavelength Shift Value (nm)
Cycle
G
CD (mdeg)
Wavelength (nm)
H
Wavelength Shift Value (nm)
Cycle

Fig. S4. Stability and durability experiment of HPC fiber

(A) CD spectrum and (B) Wavelength shift value of red fiber (T0) to yellow fiber (T2); (C) CD spectrum and (D) Wavelength shift value of red fiber (T0) to green fiber (T2); (E) CD spectrum and (F) Wavelength shift value of the red fiber (T0) to blue fiber (T2); (G) CD spectrum and (H) Wavelength shift value of green fiber (T0) to blue fiber (T2).

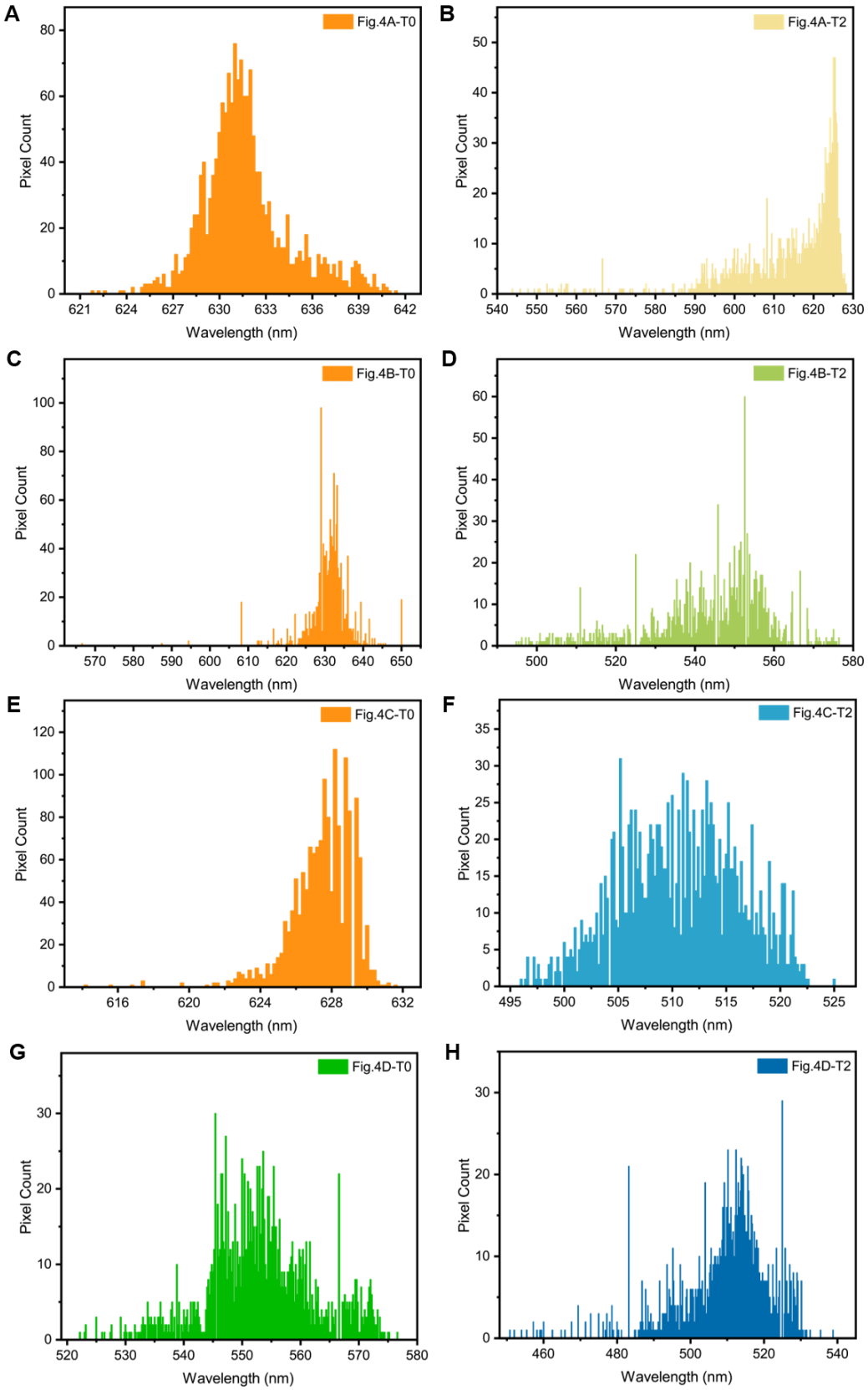

Fig. S5. Pixel-wavelength distribution histograms of HPC fibers under different background conditions in 25°C.

(A) histogram of red fiber (T0) in Figure 4A; (B) histogram of yellow fiber (T2) in Figure 4A; (C) histogram of red fiber (T0) in Figure 4B; (D) histogram of green fiber (T2) in Figure. 4B; (E) histogram of the red fiber (T0) in Figure 4C; (F) histogram of blue fiber (T2) in Figure 4C; (G) histogram of green fiber (T0) in Figure 4D; (H) histogram of the blue fiber (T2) in Figure 4D.

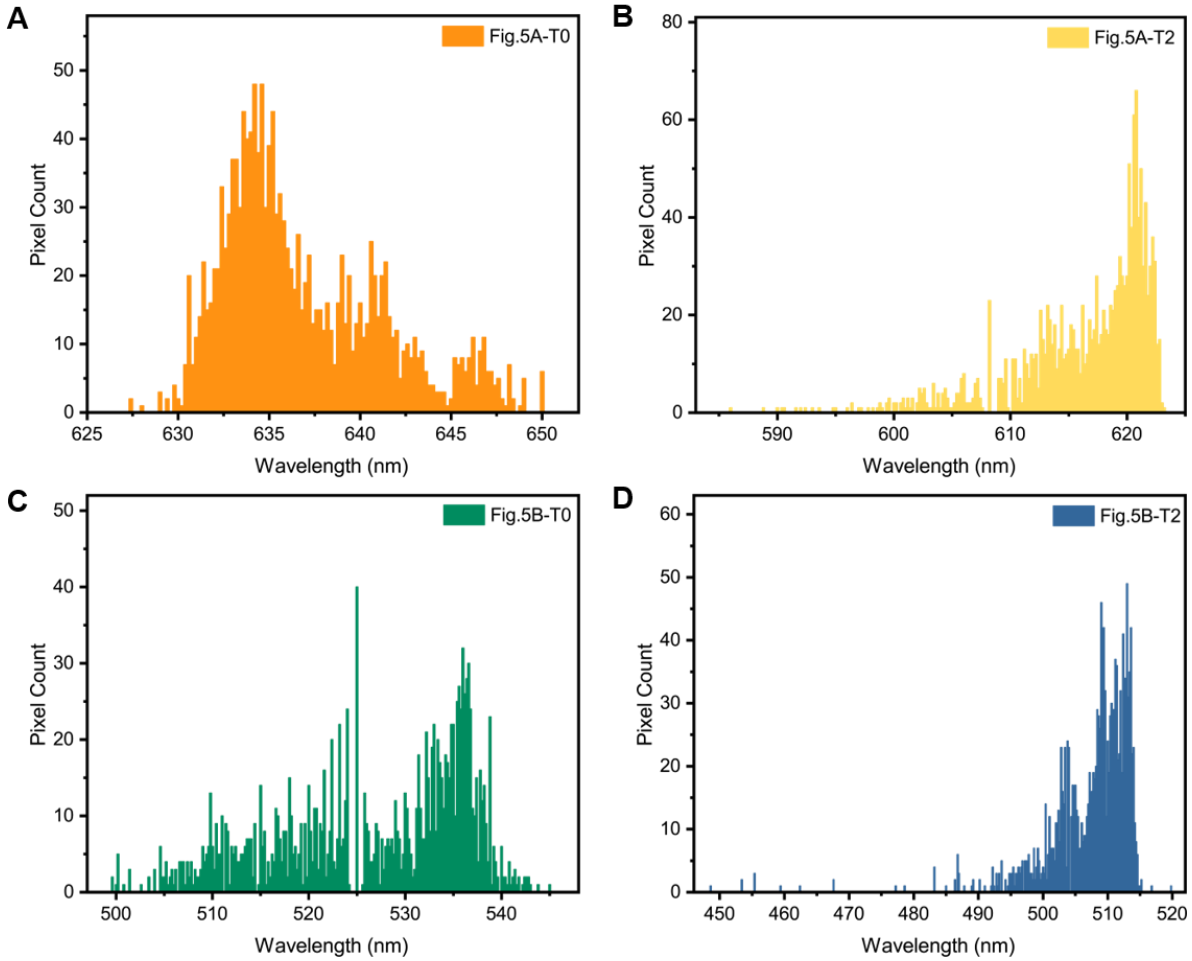

Fig. S6. Pixel-wavelength distribution histograms of HPC fibers under different background conditions.

(A) histogram of red fiber (T0) in Figure 5A; (B) histogram of yellow fiber (T2) in Figure 5A; (C) histogram of green fiber (T0) in Figure 5B; (D) histogram of blue fiber (T2) in Figure. 5B.

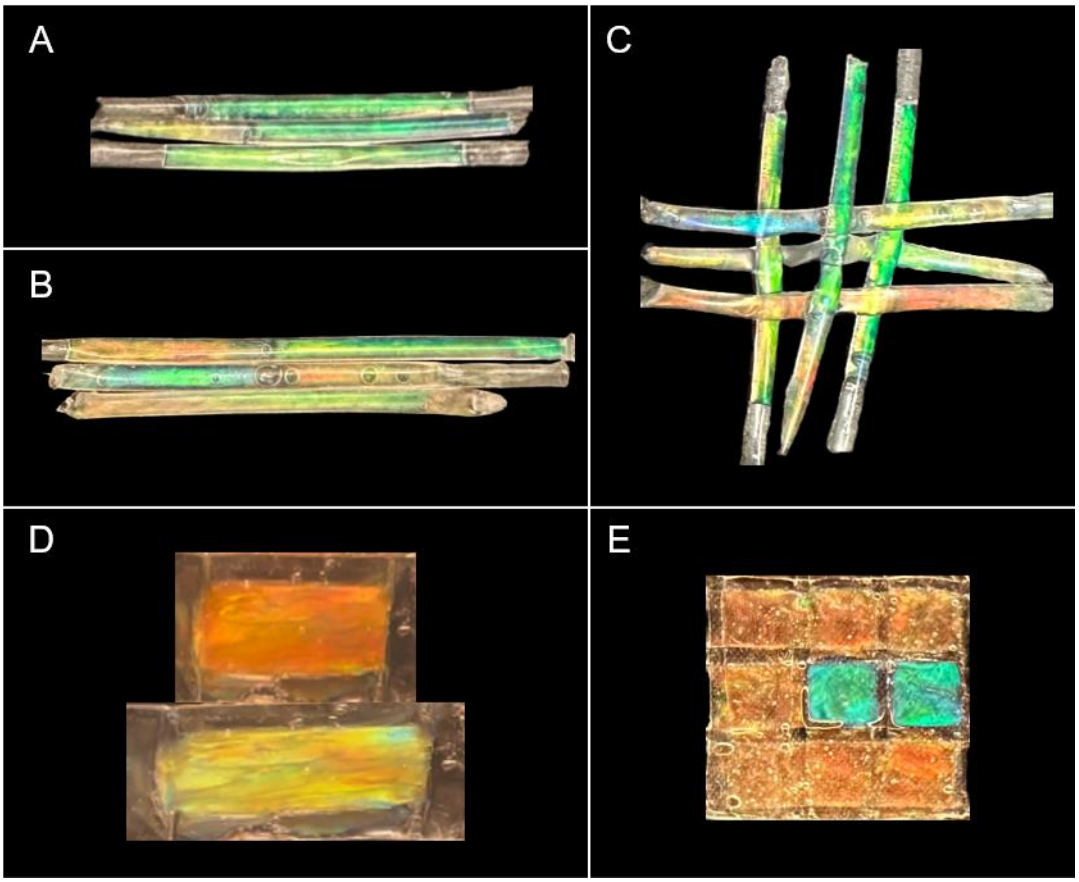

Fig. S7. Arrangement of 2D patterned HPC gels for structural color modulation.

(A) Parallel alignment of HPC fibers with uniform coloration; (B) Parallel alignment of HPC fibers with varying colors, showcasing gradient transitions; (C) Braided structure composed of HPC fibers with different colors, forming a dynamic woven network; (D) Stacked HPC membranes displaying distinct color variations at different layers; (E) Matrix-structured HPC membranes, integrating multiple color blocks for pixelated camouflage applications.

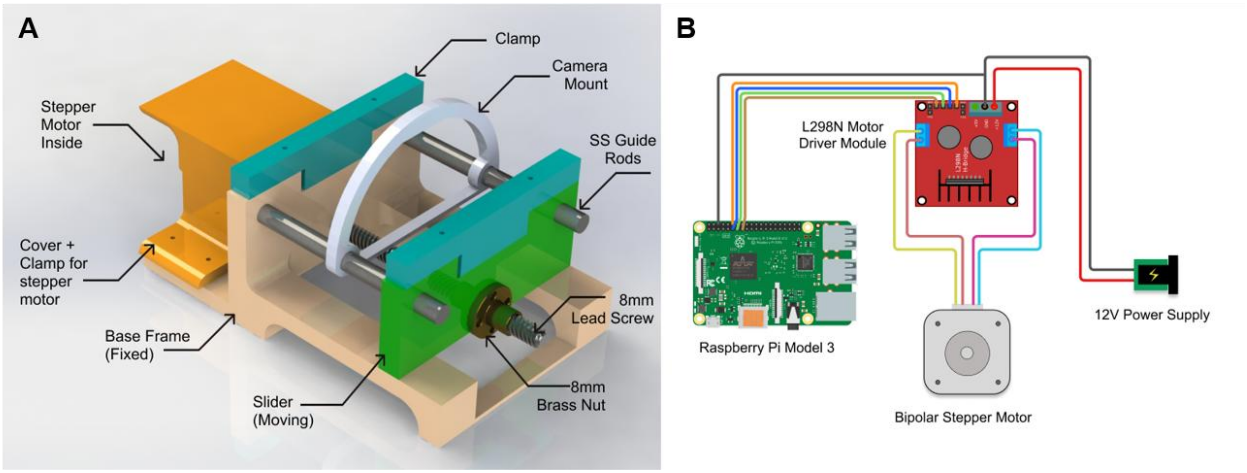

Fig. S8. Structure of the robot assembly.

(A) Mechanical components of the robot, and (B) Electrical/electronic parts of the robot.

Table S1. Hue values as well as wavelength values for various background colors and camouflaged fibers.

Background						
Color	Hue-min (°)	Hue-max (°)	Hue-ave (°)	WV-min (nm)	WV-max (nm)	WV-ave (nm)
Yellow	62.40	70.21	65.00	606.67	601.24	604.86
Green	114.39	127.20	123.31	570.56	561.67	564.37
Blue	208.92	239.04	230.22	504.92	484.00	490.12
Blue	208.19	239.04	230.23	504.42	484.00	490.12
HPC fiber						
Color	Hue-min (°)	Hue-max (°)	Hue-ave (°)	WV-min (nm)	WV-max (nm)	WV-ave (nm)
Yellow	33.91	103.33	49.77	626.45	578.24	615.44
Green	100.00	220.00	139.35	580.56	497.22	553.23
Blue	165.71	216.00	202.18	534.92	500.00	509.60
Blue	184.21	213.75	199.04	522.08	501.56	511.78

Hue-min, Hue-max, and Hue-ave mean the minimum, maximum, and average values of the hue for all pixel points in the valid picture for background and HPC fibers (T2 state), respectively. WV-min, WV-max, and WV-ave mean the minimum, maximum, and average values of the wavelength for all pixel points in the valid picture for background and HPC fibers (T2 state), respectively. The error is obtained by dividing the difference between the average wavelength of the HPC fiber and the background by the average wavelength of the background.

Table S2. Hue values and wavelength values of various background colors and camouflage fibers at different temperatures.

Background						
Color	Hue-min (°)	Hue-max (°)	Hue-ave (°)	WV-min (nm)	WV-max (nm)	WV-ave (nm)
Yellow	62.40	68.91	65.04	606.67	602.15	604.83
Blue	208.19	240.00	230.23	505.42	483.33	490.12
HPC fiber						
Color	Hue-min (°)	Hue-max (°)	Hue-ave (°)	WV-min (nm)	WV-max (nm)	WV-ave (nm)
Yellow	34.00	63.75	45.21	626.39	605.73	618.60
Blue	196.29	226.50	207.48	513.69	492.71	505.92

Hue-min, Hue-max, and Hue-ave mean the minimum, maximum, and average values of the hue for all pixel points in the valid picture for background and HPC fibers (T2 state), respectively. WV-min, WV-max, and WV-ave mean the minimum, maximum, and average values of the wavelength for all pixel points in the valid picture for background and HPC fibers (T2 state), respectively. The error is obtained by dividing the difference between the average wavelength of the HPC fiber and the background by the average wavelength of the background.

Table S3. Comparison of previous studies on chameleon-inspired robotic skin with our work.

Ref	Article title	Materials	Biodegradability
Ref.1[1]	Electrically Tunable Chameleon-Inspired Structural Colors	Liquid crystals and metallic nanostructures	Non
Ref.2[2]	Soft Stretchable Devices with Optical Color Shifting	Stretchable polymers with color-tunable layers	Non
Ref.3[3]	Magnetically Responsive Color-Shifting Soft Materials	Magnetic nanoparticles in polymer matrices	Non
Ref.4[4]	Bioinspired Soft Actuators with Tunable Optical Properties	Liquid crystal elastomers and microcapsules	Non
Ref.5[5]	Thermochromic Polymers for Adaptive Camouflage	Thermochromic pigments within polymer systems	Non
Ref.6[6]	Smart Hydrogel Materials for Robotics	Synthetic hydrogel with mechanical and optical properties	Non
Ref.7[7]	Light-Driven Artificial Skin for Robotics	Photo-responsive polymers and pigments	Non
Ref.8[8]	Nanostructured Materials for Color-Changing Robotics	Metal nanostructures embedded in elastomers	Non
Ref.9[9]	Photonic Crystal-Based Structural Color Materials	Gold nanorods and photonic crystals	Non
This work	Force-Induced Color Change Smart Textile	Hydroxypropyl cellulose	Highly degradable

Movie S1

Manual demonstration of reversible stretching of HPC fiber.

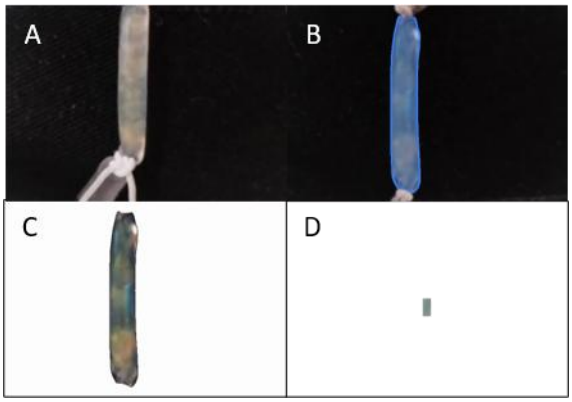

We provide supplementary HPC robot videos named in the format Movie S{num}-{letter}, where the number 2, 3, 4, 5, 6, and 7 denote different video segments for each experiment, and the letter a, b, c, d, and e represent different components of the processed videos.

Movie S*-a (*: from 2 to 7)

HPC Fiber Reversible Stretching Demonstration: This video, captured directly by the camera installed on the robot, shows the real-time status of the fiber as it undergoes stretching by the motor.

Movie S*-b (*: from 2 to 7)

Ego-Robots & Environmental Background Pixel Segmentation Demonstration: This video provides a segmentation map of the original camera-captured footage, splitting frame pixels into fiber as the foreground and environment pixels as the background.

Movie S*-c (*: from 2 to 7)

Foreground Pixels: This segment demonstrates the dynamic segmentation of foreground pixels, highlighting changes in fiber pixels during the stretching process.

Movie S*-d (*: from 2 to 7)

Traditional Approach Using a Predefined Bounding Box or Color Sensors: This video compares our method with traditional approaches by segmenting a fixed area of pixels to represent the limited reception field of color sensors, showing how they shift as the motor operates.

Movie S*-e (*: from 2 to 7)

Background Pixels: This segment displays the segmented environmental background pixels during the stretching process, highlighting changes in the background segmentation.

These supplementary videos provide a comprehensive view of the robotic fiber's dynamic behavior, illustrating how our segmentation and control methods outperform traditional approaches.

References:

(1) Chou, H.-H.; Nguyen, A.; Chortos, A.; To, J. W. F.; Lu, C.; Mei, J.; Kurosawa, T.; Bae, W.-G.; Tok, J. B.-H.; Bao, Z. A Chameleon-Inspired Stretchable Electronic Skin with Interactive Colour Changing Controlled by Tactile Sensing. *Nat Commun* **2015**, *6* (1), 8011. https://doi.org/10.1038/ncomms9011.

(2) Kim, H.; Choi, J.; Kim, K. K.; Won, P.; Hong, S.; Ko, S. H. Biomimetic Chameleon Soft Robot with Artificial Crypsis and Disruptive Coloration Skin. *Nat Commun* **2021**, *12* (1), 4658. https://doi.org/10.1038/s41467-021-24916-w.

(3) Zhang, W.; Tian, H.; Liu, T.; Liu, H.; Zhao, F.; Li, X.; Wang, C.; Chen, X.; Shao, J. Chameleon-Inspired Active Tunable Structural Color Based on Smart Skin with Multi-Functions of Structural Color, Sensing and Actuation. *Materials Horizons* **2023**, *10* (6), 2024–2034. https://doi.org/10.1039/D3MH00070B.

(4) Wu, Y.; Wang, Y.; Zhang, S.; Wu, S. Artificial Chameleon Skin with Super-Sensitive Thermal and Mechanochromic Response. *ACS Nano* **2021**, *15* (10), 15720–15729. https://doi.org/10.1021/acsnano.1c05612.

(5) Hu, Y.; Wei, B.; Yang, D.; Ma, D.; Huang, S. Chameleon-Inspired Brilliant and Sensitive Mechano-Chromic Photonic Skins for Self-Reporting the Strains of Earthworms. *ACS Appl. Mater. Interfaces* **2022**, *14* (9), 11672–11680. https://doi.org/10.1021/acsami.2c00561.

(6) Li, L.; Li, H.; Cao, J.; Li, S. Heat Transfer Characteristics of the Microfluidic Biomimetic Chameleon Skin with Active Thermal Camouflage. *J Bionic Eng* **2023**, *20* (2), 722–733. https://doi.org/10.1007/s42235-022-00286-x.

(7) Chen, R.; Chen, J.-Q.; Sun, Y.; Wu, L.; Guo, J.-L. A Chameleon Tongue Inspired Shooting Manipulator With Vision-Based Localization and Preying. *IEEE Robotics and Automation Letters* **2020**, *5* (3), 4923–4930. https://doi.org/10.1109/LRA.2020.3005128.

(8) Dong, Y.; Bazrafshan, A.; Pokutta, A.; Sulejmani, F.; Sun, W.; Combs, J. D.; Clarke, K. C.; Salaita, K. Chameleon-Inspired Strain-Accommodating Smart Skin. *ACS Nano* **2019**, *13* (9), 9918–9926. https://doi.org/10.1021/acsnano.9b04231.

(9) Wang, Y.; Cui, H.; Zhao, Q.; Du, X. Chameleon-Inspired Structural-Color Actuators. *Matter* **2019**, *1* (3), 626–638. https://doi.org/10.1016/j.matt.2019.05.012.